DYNAMICS OF RIPARIAN SALTWATER INTRUSION IN URBAN STREAMS

by
Emily Rose Fedders

Honors Thesis

Appalachian State University

Submitted to the Department of Geological and Environmental Sciences
and The Honors College
in partial fulfillment of the requirements for the degree of
Bachelor of Science

May, 2019

Approved by:

William P. Anderson, Jr., Ph.D., Thesis Director

Bob Swarthout, Ph.D., Second Reader

Cole Edwards, Ph.D., Departmental Honors Director

Jefford Vahlusch, Ph.D., Dean, The Honors College

ABSTRACT

Accumulation of road salt in stream and groundwater approaching or exceeding salinity tolerances of aquatic life and recommendations for healthy drinking water is well documented across cold regions of the US and elsewhere. However, mechanisms by which salt enters groundwater, from where it contributes to long-term contamination of surface water, are less understood. Here we utilize groundwater flow models based on field observations at two study sites to investigate the efficacy of near-stream reverse gradients created by elevated stream stage during storm and runoff events as one such forcing mechanism for salt plume intrusion into the near-stream aquifer. Our study sites are located on Boone and Hardin Creeks, small mountain streams located in the headwaters of the New River watershed in the town of Boone, NC, USA, which exhibit year-round stream salinities near 0.2‰ as well as acute spikes in salinity up to 9‰ in winter months. Two model domains, with 1 m and 2 m thick floodplain permeable layers, respectively, based on observed stream channel geometry were constructed for each site, for a total of four model scenarios. Observations of stream stage and salinity at these sites informed synthetic stream boundary conditions for the models. These model scenarios allow us to build upon previous work in comparing the combined effects of stream channel size and morphology, permeable layer thickness, and storm flashiness on the efficacy of salt plume intrusion. We find storm-induced reverse gradients are indeed an effective mechanism at introducing salt to the floodplain aquifer, in agreement with previous work. Additionally, we find that salt accumulation in the aquifer follows a logarithmic trend and that the flashier nature of smaller streams promotes more effective aquifer salinization, while a thinner aquifer promotes more efficient salt export by preventing the salt plume from spreading, thus keeping baseflow salt concentrations high.

Keywords: *road salt, aquifer salinization, urban watershed, salt plume intrusion*

CONTENTS

1 INTRODUCTION

Since the mid-1900s, application of road salt (primarily NaCl) to impervious surfaces for the improvement of winter road and sidewalk safety has become increasingly popular in the United States (US) (Godwin et al., 2002), with a total of 22.7 Mt of road salt applied across the US in 2015 (USGS,2015). Long-term increases in Cl^- and Na^+ concentrations in both groundwater (Cooper et al., 2014; Perera et al., 2013; Novotny et al., 2009; Williams et al., 2000) and surface water (Corsi et al., 2015; Likens et al., 2009; Kelly et al., 2008; Kaushal et al., 2005; Godwin et al., 2002) have been well documented in developed areas across the northeastern US and Canada since the 1950s. While road salt is not the only possible source of urban Cl^-, wastewater treatment facilities can also be point sources of Cl^- contamination, 70%-91% of Cl^- introduced to the environment in urban areas comes from road salt (Novotny et al., 2009; Kelly et al., 2008). Further supporting the link between road salt and watershed salinization, Corsi et al. (2015) and Kaushal et al. (2005) show watershed salinization increases logarithmically with increasing area of impervious surface coverage (ISC).

During winter melt or rain events, this salt spread on impervious surfaces either runs off into surface water bodies or infiltrates into groundwater (Snodgrass et al., 2017; Perera et al., 2013). Mass balance computations indicate between 16.3% and 70% of this annual anthropogenic salt load to urban watersheds is stored locally in groundwater, ponds, and wetlands, leading to accumulation of salt mass over time (Perera et al., 2013; Novotny et al., 2009). Urban streams exhibit baseflow salinities elevated above those observed in nearby undeveloped watersheds (Cooper et al., 2014; Kaushal et al., 2005; Kunkle, 1972), and groundwater Cl^- concentrations exceed concentrations in less-developed areas by an order of magnitude (Williams et al., 2000). Snodgrass et al. (2017) and Godwin et al. (2002) observe molar Na^+:Cl^- ratios near 1 as expected from dissolution of NaCl in winter streamflow immediately following melt events, but much lower ratios during

summer baseflow conditions, indicating Na^+ has had opportunity to participate in cation exchange with soils. Combined, the observations discussed above all point to groundwater as a reservoir for salt on at least yearly timescales.

This widespread increase in watershed salinity and accumulated salt mass is cause for both ecological and human health concern. The chronic (four-day running average) ambient water quality criteria for aquatic life for Cl^- concentration suggested by the United States Environmental Protection Agency (USEPA) is 0.23‰ (USEPA, 1988), which is regularly approached or exceeded in urban streams (Cockerill et al., 2017; Snodgrass et al., 2017; Kaushal et al., 2005). Mortality limits for acute (24 to 96 hour) exposure periods are higher, ranging from 20‰ for some trout species (Wagner et al., 2001), 8‰ to 10‰ for various invertebrate species (Berezina, 2002; Blasius et al., 2001), 2.9‰ for fathead minnows (Corsi et al., 2010), and 1‰ for American woodfrogs (Gallagher et al., 2014). However, these studies agree stress responses such as failure to eat or breed are exhibited below these extreme upper thresholds. Salinization of human drinking water is also a potential threat, as ground and surface waters near population centers in the northeastern US exhibit Cl^- concentrations up to 25% that of seawater (8.75‰) (Kaushal et al., 2005), well above the USEPA secondary drinking water standard for Cl^- of 0.25‰ (USEPA, 2018).

In short, there is consensus that road salt accumulates in groundwater in developed watersheds. This accumulation creates year-round elevated salinity conditions in both surface water and groundwater, which can adversely affect aquatic life and has the potential to detrimentally affect human health as well. The less studied issue is the mechanism by which salty water enters urban groundwater. Understanding what controls whether salt leaves the local system or remains and accumulates is important to understanding how to better manage stormwater runoff in urban areas to reduce this phenomenon of watershed salinization.

Ledford et al. (2016) propose infiltration of stormwater to the floodplain during over-

bank events as the primary mechanism for salt entry into groundwater. Modeling and observations by Snodgrass et al. (2017) show that stormwater retention ponds, by fulfilling their purpose and allowing stormwater infiltration, create groundwater salt plumes which contribute significantly to summer baseflow salinity in nearby streams. These and others (Snodgrass et al., 2017; Ledford et al., 2016; Kelly et al., 2008) assume that any salt which reaches a stream and is not discharged to the floodplain in an overbank event is evacuated from the local system. Cockerill et al. (2017), working in the same watershed as this study, offer the alternative hypothesis that near-stream reverse hydraulic gradients during periods of elevated stream stage are effective at salinizing the floodplain aquifer without ponding or overbank events. Reverse gradients during storm events are a frequent stream condition common to watersheds with varying degrees of urbanization and stormwater management infrastructure. In the work presented here, we further explore this mechanism since the frequency and commonality of reverse hydraulic gradient events give them potential importance not only to our study system, but also to a diversity of other watersheds.

With this previous work in mind, the goals of this study are twofold. We re-investigate the findings of Cockerill et al. (2017) with the addition of new data, more detailed modeling, and an additional study site, in order to increase understanding of the effects of streambed morphology, flashiness, permeable layer thickness, and storm salinity on salt storage and discharge. Additionally, we explore whether the system we observe has yet reached a steady state of salt mass accumulation, or if we can expect summer baseflow stream salinities to continue to increase.

2 METHODS

2.1 Study Area

To accomplish these objectives, we develop two two-dimensional cross-sectional model domains based on the geometries and hydraulic conditions observed at two long-term

monitoring sites: site BC, on Boone Creek (also the site of the Cockerill et al., 2017 study), and site HC, on Hardin Creek. Both study streams are mountain headwater streams of the New River watershed, located in Boone, North Carolina, USA (Fig. 1).

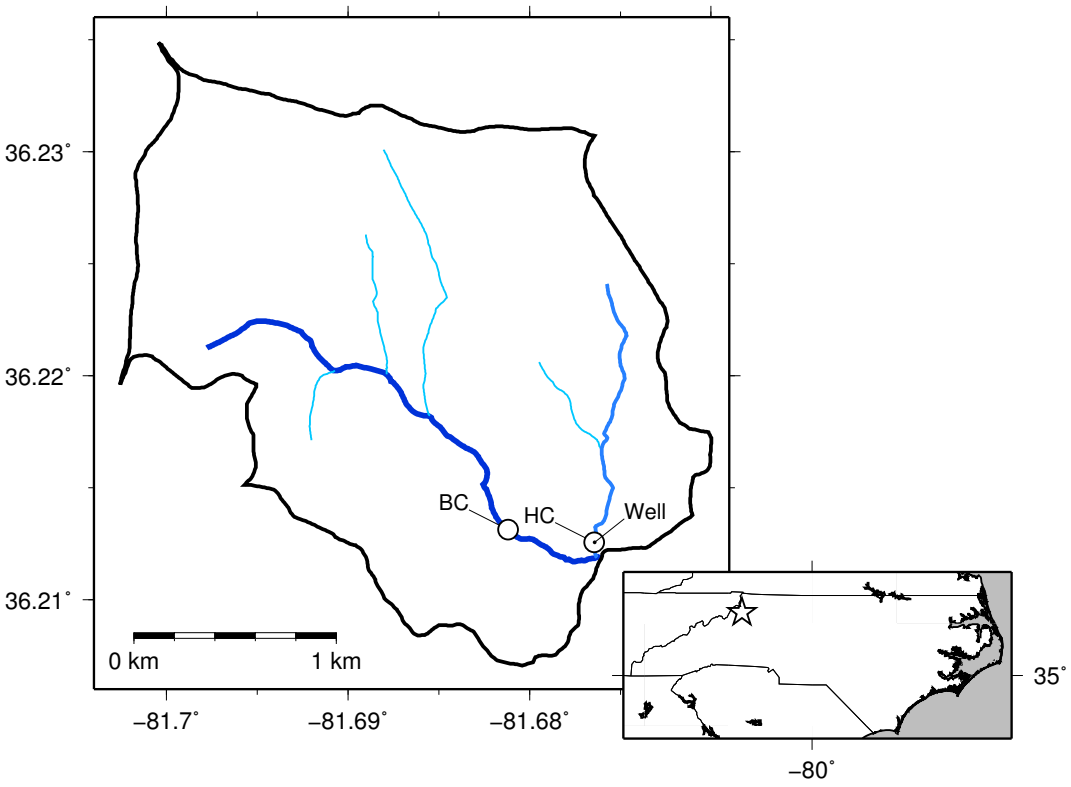

Figure 1: The Boone Creek study watershed (heavy black line) located in Boone, North Carolina, USA (inset map). Boone Creek (BC) and Hardin Creek (HC) monitoring sites are marked with circles. The black dot marks the streambank monitoring well. The watershed boundary ranges in elevation from 1438m at the northwest corner to 963m at the outlet.

Boone Creek is a low-to-moderate gradient stream extending 2.10 km upstream of site BC, which marks the outlet of a 3.78km^2 catchment area. Hardin Creek is a moderate-gradient, lower-discharge tributary which joins Boone Creek downstream of site BC. Site HC, located just upstream of this confluence, drains a 1.47km reach and 1.25km^2 sub-catchment of the greater Boone Creek watershed.

Figure 2: Liberal salting on the campus of Appalachian State University in Boone, NC, USA.

Both streams flow through developed environments including residential areas, a downtown shopping district, and the campus of Appalachian State University. The stream reach above BC has 52.4% ISC in the riparian corridor extending 100m on either side of the channel. The reach above HC has 33.7% ISC in the 100m riparian corridor. Salt is applied liberally to these impervious surfaces during the winter months (Fig. 2), when spikes in salinity greater than 9‰ (HC) and 5‰ (BC) have been observed in-stream during runoff events (Fig. 3,4). Observed stream salinities remain near 0.2‰ even in summer when salt has not been applied to nearby ISC in months. These baseflow values approach and sometimes exceed the USEPA suggested chronic ambient freshwater Cl^- content of 0.23‰ (USEPA, 1988) as well as the secondary drinking water standard for Cl^- of 0.25‰ (USEPA, 2018). While these standards are for Cl^- and not total salinity, ion chromatography (IC) analysis of water samples taken from Boone and Hardin Creeks indicate Cl^- is the main contributor to stream salinity, providing between 71% and 93% of total sample salinity on average.

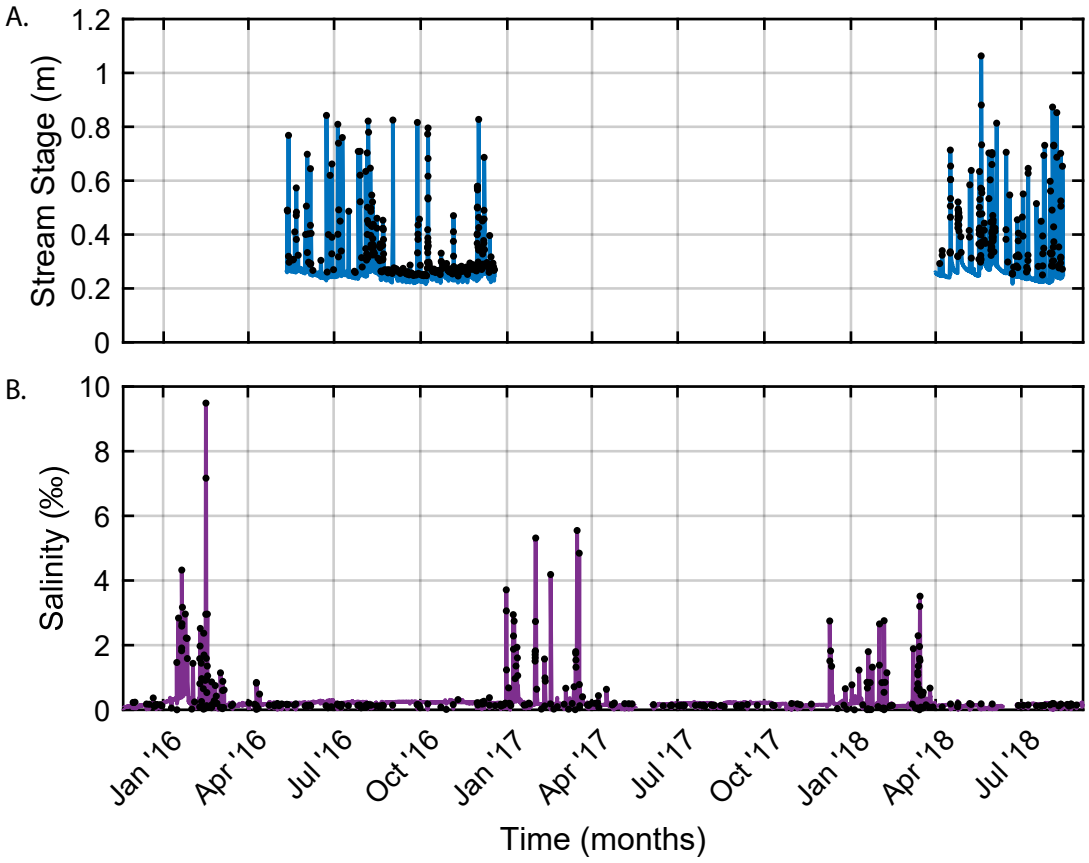

Figure 3: A) Observed stage, and B) salinity time series for site BC (solid line), with USEPA chronic water quality recommendation for Cl^- (0.23‰) (USEPA, 1988). Fluctuation peaks picked by the findpeaks algorithm are marked with black dots. Summer baseflow salinity remains near 0.15‰. Gaps in data are due to lost or malfunctioning loggers, or transitions in logging schemes.

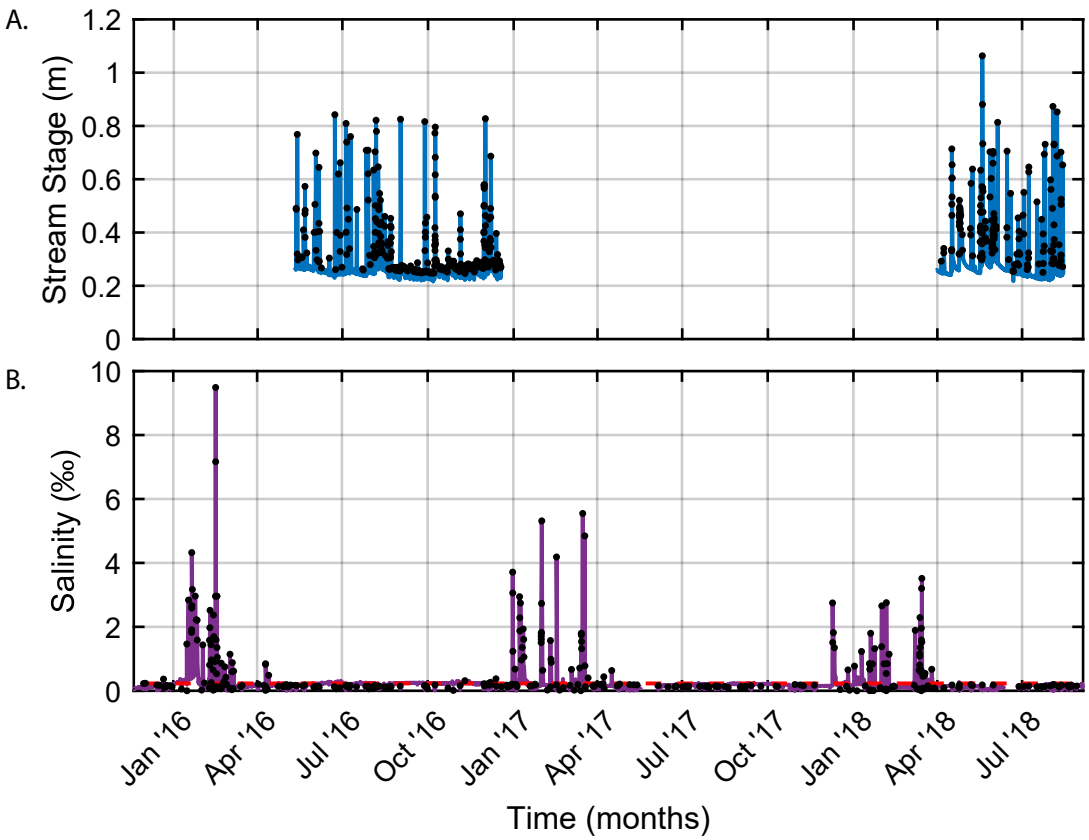

Figure 4: A) Observed stage, and B) salinity time series for site HC (solid lines), with USEPA chronic water quality recommendation for Cl^- (0.23‰) (USEPA, 1988).. Fluctuation peaks picked by the findpeaks algorithm are marked with black dots. Summer baseflow salinity remains near 0.22‰. Gaps in data are due to lost or malfunctioning loggers, or transitions between logging schemes.

Salinity time series from a monitoring well installed in the Hardin Creek floodplain 1m from the streambank at site HC generally mimic the in-stream signal with muting and lag (Fig. 5). This monitoring well is unfortunately screened through the ground surface, allowing fresh runoff to enter from the top and adulterate the groundwater signal, which leads to the extreme freshening events observed in the well time series. Despite this freshening contamination, down-well salinities exceed in-stream salinities in summer months, pointing to groundwater as a source of salt to the stream during those times.

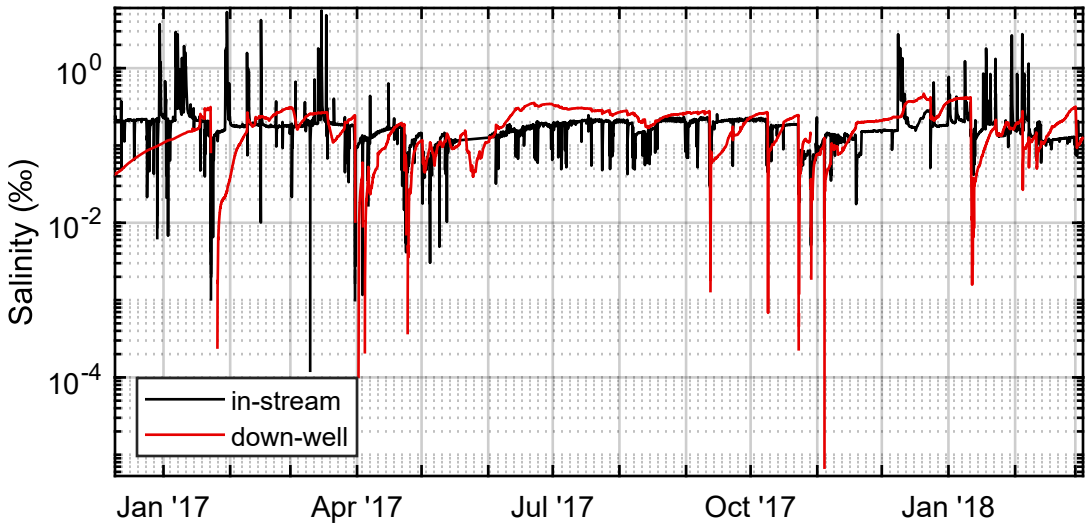

Figure 5: Salinity time series calculated from observed conductivity in Hardin Creek at site HC (black line) and a monitoring well in the adjacent floodplain (red line). The groundwater signal is muted, but exhibits both freshening and salinization events. Extreme freshening is due to surface water contamination of the well during freshwater runoff events, since the well is screened through the ground surface

2.2 Data Collection

2.2.1 Stage

36 months of stream stage data between 2013 and 2018 were collected at site BC, and 15 months of stream stage data between 2016 and 2018 were collected at site HC. These data were collected using a variety of data loggers deployed both in stream and in stilling wells as outlined in table 1. Barometric pressure, P_b, calculated from altimeter setting (eq. 1) data obtained from the North Carolina Climate Office weather station KTNB located 2.75 km from the study site, was subtracted out of logged pressure time series from unvented stage loggers to obtain the portion of the signal due to stream stage fluctuations rather than air pressure changes.

$$P_b = \left(A^b - ah\right)^{1/b} + 0.3 \tag{1}$$

A is altimeter setting in mb, h is weather station elevation = 910.4m, and a and b are constants equaling $8.42288\text{E}^{-0.5}$ and 0.190284, respectively.

Site	*Dataset*	*Instrument*	*Instrument Precision*	*Deployment method*
BC	Stage (unvented)	In-Situ Level TROLL 700	+/- 0.05% of full span	Stilling well
BC	Stage (vented)	HOBO MX2001-04	+/- 0.075% or 0.3cm	Stilling well
BC	Stage	Stevens T-SDX-93720	+/- 0.25% of full span	Stilling well
BC	Conductivity	HOBO U24-001	3% of reading or 5µS/cm	In-stream
HC	Stage (unvented)	HOBO U20L-04	+/- 0.1% or 0.8cm	In-stream
HC	Stage	Stevens T-SDX-93720	+/- 0.25% of full span	Stilling well
HC	Conductivity	HOBO U24-001	3% of reading or 5µS/cm	In-stream

Table 1: Stage and salinity logging schemes at sites BC and HC.

2.2.2 Salinity

Stream conductivity as a proxy for salinity was logged at both sites at 15-minute intervals using HOBO U24-001 freshwater conductivity data loggers deployed in-stream. The conductivity loggers were tied to stakes driven into the streambed and floated with four-inch sections of pipe insulation to prevent sediment burial of the logger without obstructing the sensor.

Additional conductivity measurements were taken at times of data logger offload and re-launch using a Yellow Springs Instruments (YSI) 556 MPS handheld sampler. These measurements were used as endpoints for drift correction of the logged conductivity time series. Drift-corrected conductivity data were converted empirically to salinity using eq. 2-4 after Fofonoff and Millard (1983).

$$S = a_0 + a_1 R_T + a_2 R_T + a_3 R_T^{3/2} + a_4 R_T^2 + a_5 R_T^{5/2} + \Delta S \tag{2}$$

$$\Delta S = \frac{T-15}{1+k(T-15)}\left(b_0 + b_1 R_T^{1/2} + b_2 R_T + b_3 R_T^{3/2} + b_4 R_T^2 + b_5 R_T^{5/2}\right) \quad (3)$$

$$R_T(S,T) = \frac{C(S,T,0)}{C(35,T,0} \quad (4)$$

$C(35,T,0)$ is a reference value for conductivity of seawater with salinity equal to 35‰ at temperature, T, and atmospheric pressure. $C(S,T,0)$ is the observed conductivity at unknown salinity S taken at temperature T and atmospheric pressure. a_i, b_i, and k are constants defined as follows:

a_0 = 0.0080	a_4 = -7.0261	b_2 = -0.0066	k = 0.01
a_1 = -0.1692	a_5 = 2.7081	b_3 = -0.0375	
a_2 = 25.3851	b_0 = 0.0005	b_4 = 0.0636	
a_3 = 14.0941	b_1 = -0.0056	b_5 = -0.0144	

These empirically-determined salinity values were checked against the sum of the concentrations of seven anions (F^-,Cl^-,NO_2^-, BrO_2^-, NO_3^-, PO_4^{-3}, and SO_4^{-2}) obtained by ion chromatography analysis of 39 water samples taken from 10 sites in the Boone Creek watershed (including HC and BC) using a Dionex ICS-1600 ion chromatography unit with Chromeleon CDS processing software (Fig. 6)

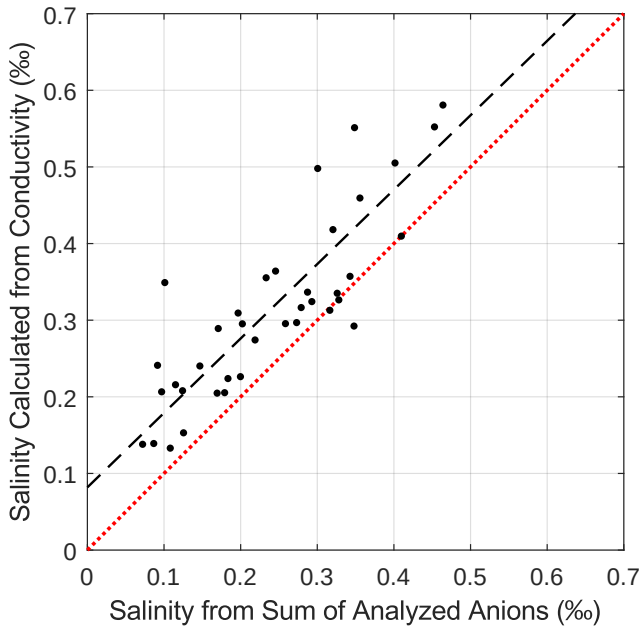

Figure 6: Calculated salinity plotted against salinity from sum of F^-,Cl^-,NO_2^-, BrO_2^-, NO_3^-, PO_4^{-3}, and SO_4^{-2} content as determined by IC analysis. The black dashed line is the least squares linear regression fit to the plotted data ($Sal_{calc} = 0.971 * Sal_{sum} + 0.082$,$R^2 = 0.773$). The red dotted line is the 1:1 line that would be expected if the salinity calculation were accurate and the analyzed ions are the only ions present.

The calculated and measured datasets showed good correlation with an R^2 value of 0.77 (eq. 5). Calculated salinity values from measured conductivity exceeded salinity measured by IC by an average of 0.075‰ but the slope of the least squares linear regression fit to the two datasets was 0.971, near the expected slope of 1. It is reasonable that there would be more ions in the stream water than the seven measured via IC, so we took the good correlation and near-one slope as evidence of the empirical method being a reasonable estimate of salinity despite this overshoot.

$$R^2 = 1 - \frac{\sum_{n=1}^{n}(y_n - \hat{y}_n)^2}{\sum_{n=1}^{n}(y_n - \bar{y})^2} \tag{5}$$

y_n is observed data, $\hat{y_n}$ is modeled data, and $\bar{y}$ is the mean of the observed data.

2.2.3 Grain Size Distribution and Hydraulic Conductivity

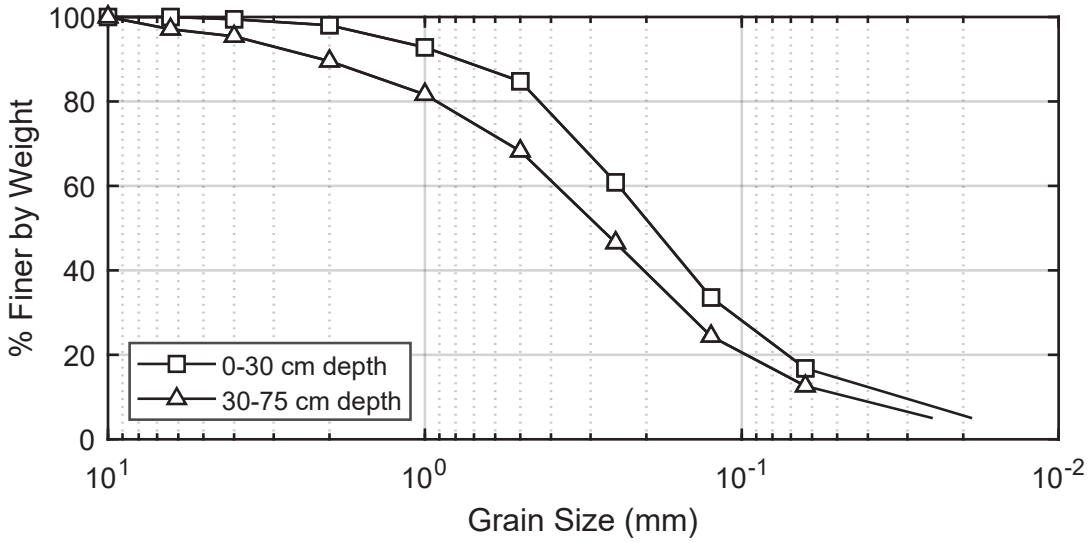

Figure 7: Grain-size distribution for sediment samples collected from the Hardin Creek floodplain 1m from stream bank. Sediment fines with depth, but effective grain size, d_{10}, which 10% of the sample is finer than, is similar between the two samples. Thus the average d_{10} was used in floodplain hydraulic conductivity calculations.

Two sediment samples were obtained from the streambank, one from 0-30 cm depth and one from 30-75 cm depth, using a tubular soil sampler. These samples were dried and sieved to determine the grain size distribution curve (Fig. 7) and effective grain diameter, d_{10} for estimation of representative floodplain aquifer hydraulic conductivity, k, by the Hazen formula (eq. 6).

$$k = Cd_{10}^2 \tag{6}$$

k was determined to be 1.618m/d using $C = 100\text{cm}^{-1}s^{-1}$ and d_10=0.0437mm.

2.3 Data Analysis

Observed time series of stage and salinity at both sites were processed using the `findpeaks` function in Matlab matrix algebra software to obtain the magnitude, duration (half-life), and inter-event time, of stage and salinity fluctuations at each study site (Fig. 3,4). The search for stage fluctuations was limited to those greater than 2cm of

prominence. The search for salinizing salinity fluctuations was limited to 0.3‰ prominence, and for freshening salinity events to 0.1‰ negative prominence. These attributes were visually determined to exhibit log-normal distributions (Fig. 8).

2.4 Synthetic Data Generation

The mean and standard deviation of the logarithm of storm attribute data were used to generate attributes for synthetic storms following the same log normal distributions as the observed data for use in the models described in section 2.5 below. Generated attributes were curated before being used to compile synthetic time series as follows:

For stage attributes, generated fluctuation magnitudes less than 2cm were discarded for both BC and HC synthetic time series, as no peaks below 2 cm prominence were pulled from the observed data. Fluctuation magnitudes greater than 1.5m were discarded from the generated attributes for HC, and greater than 2.0 were discarded from generated attributes for BC, as these were seen as unrealistic except in rare cases. Interstorm times greater than 21 days were discarded to prevent generation of anomalous drought conditions. Event durations and interstorm times less than 15 minutes were discarded to avoid overinterpretation of our 15 minute resolution observed data.

For salinity attributes, generated salt peak magnitudes less than 0.3‰ were discarded for both site models, because no peaks less than this were pulled from the observed data. All freshening attributes were kept. Interstorm times were not generated for salinity or freshening events, as these always correspond with stage fluctuations.

Synthetic stage time series (Fig. 9) were then generated according to the following steps:

1. Cumulatively sum interstorm times to obtain sequential fluctuation peak times.

2. Generate individual storm pulses, $X(t)$, at each storm time, t_s, using generated

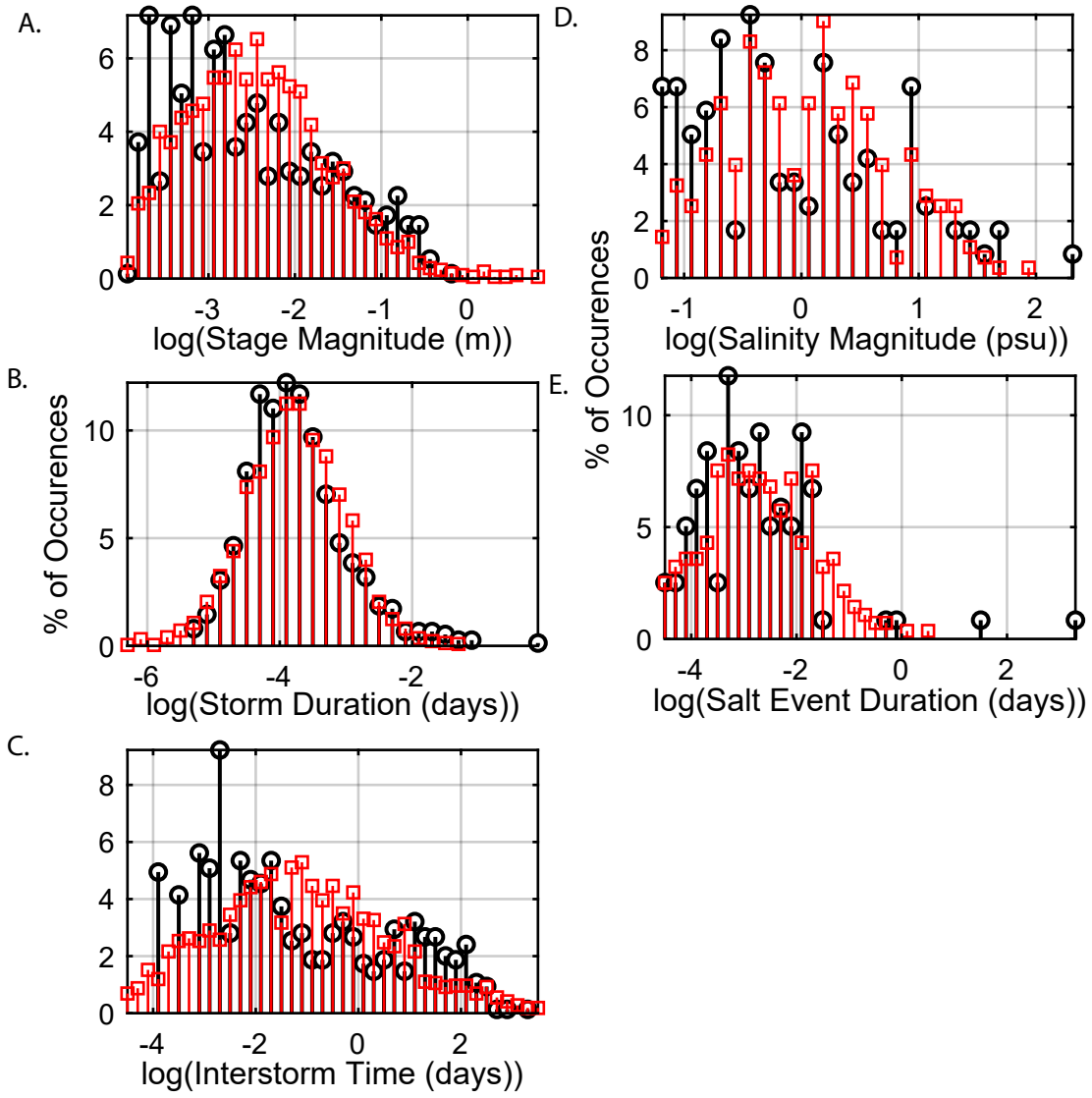

Figure 8: Distribution of the log of observed (black circles) and generated (red squares) storm attributes: stage fluctuation magnitude (A), stage fluctuation duration (B), time between storms (C), salinity fluctuation magnitude (D), and salt fluctuation duration (E) for HC. The same analysis was performed for site BC as well. Interstorm time was not analyzed for salt events, since salt fluctuations must happen concurrently with stage fluctuations.

peak magnitudes, M, and durations, D, in an exponential decay function (eq. 7).

$$X(t) = M * 0.5\frac{t - t_s}{D} \tag{7}$$

3. Sum storm pulses that overlap in time to obtain a total synthetic time series.

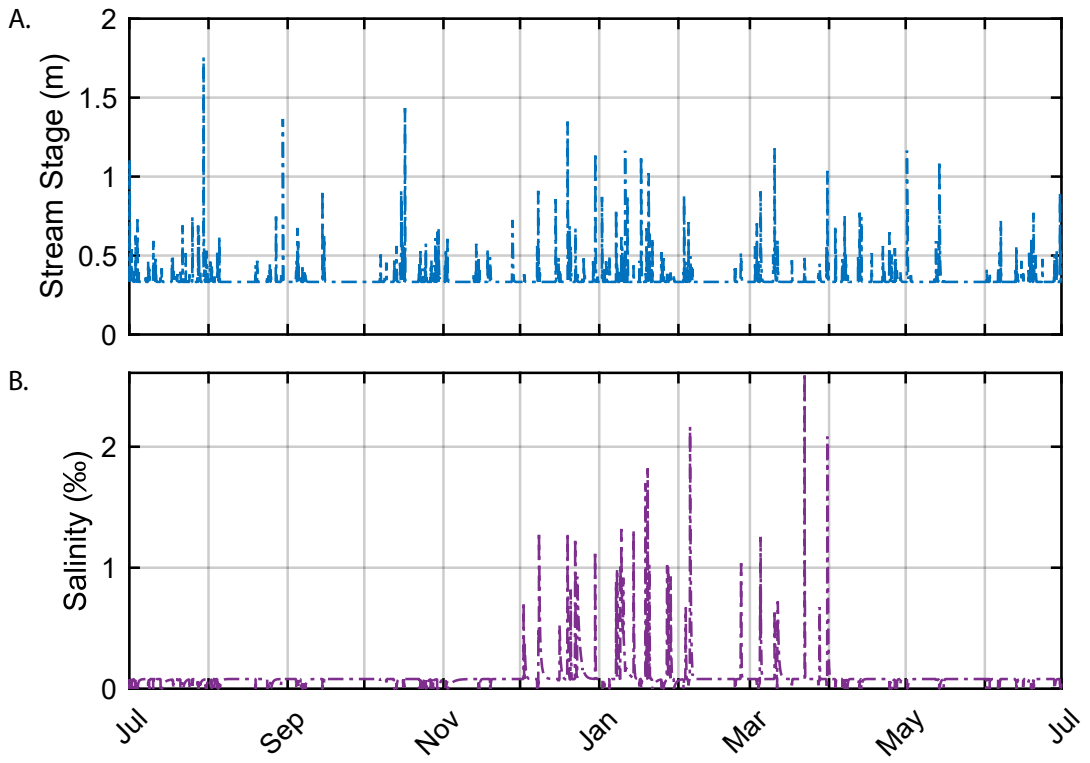

Figure 9: A) Example synthetic stage and B) salinity time series generated for site BC for a single model year with baseline salinity set to 0.08‰. Each stage peak has a corresponding salinity fluctuation, either freshening or salinizing.

Synthetic salinity time series were generated next as follows:

1. Pull 40 random stage fluctuation times from the winter period (model days 154 to 274 for our July 1 to June 30 model years).

2. Create salinity pulses at those 40 random times using generated salinity event M and D in eq. 7.

3. Generate freshening pulses at each of the remaining stage fluctuation event times, again using eq. 7.

4. Sum salinization and freshening time series to obtain a total time series.

5. Add desired baseline salinity to the combined time series.

6. Constrain minimum salinity time series value to be zero.

We tested the efficacy of this method of modeling stage and salinity event pulses as exponential decay functions by generating salinity time series to match the observed data from the BC site (Fig. 10). The error between the observed and generated time series was determined by comparing the numeric integrals of the two time series. The %error (eq. 8) between the observed and generated stage time series was 7.57%. The %error between the area under the observed and generated salinity time series was 19%.

$$\%error = \mid \frac{observed - synthetic}{observed} \mid *100 \tag{8}$$

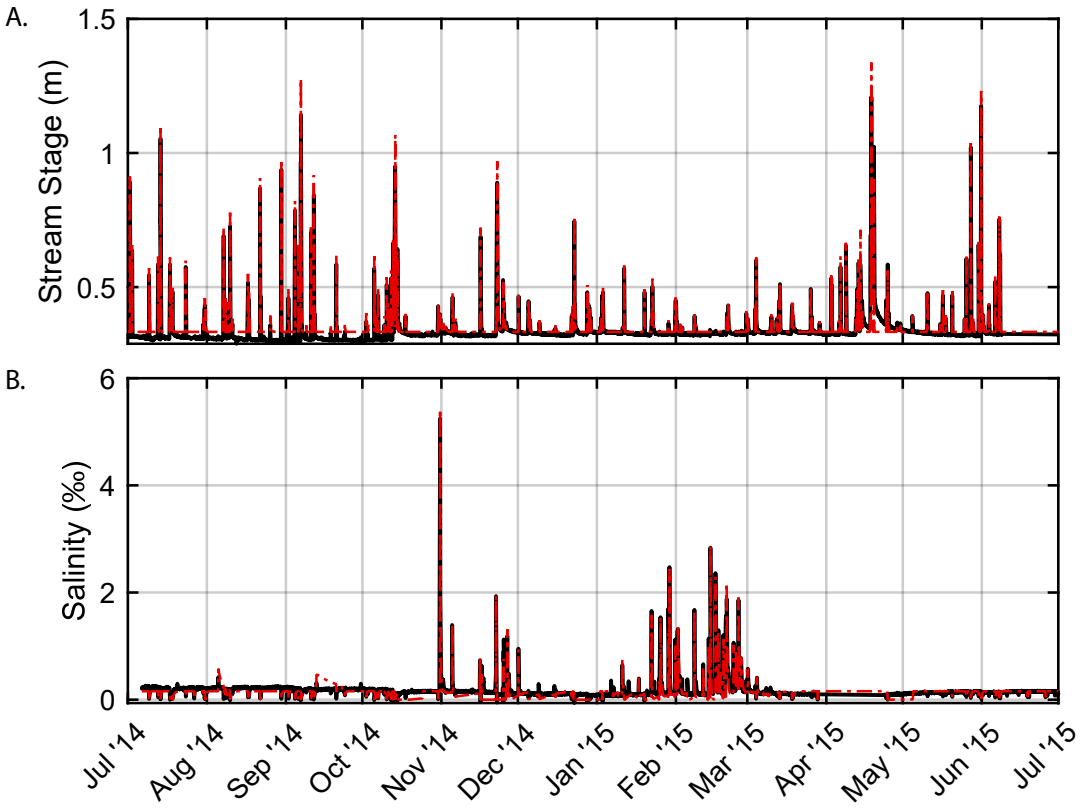

Figure 10: A) observed stage (black line), and B) observed salinity (black line) time series excerpted from BC data, shown with synthetic time series (dashed red line) generated to match the observed data using exponential functions with timing, magnitude, and duration determined by findpeaks to approximate the storm pulses. The synthetic data agrees well with the observed data.

2.5 Models

2.5.1 Domain

The domain for each site model was constructed in Feflow7.1 finite-element groundwater flow and solute transport modeling software as a half cross-section perpendicular to the stream channel and extending 50m into the floodplain. Coordinates for the upper boundary of the model domain were developed from cross-sectional surveys conducted at the two study sites combined with elevations taken from cross-stream transects drawn in Google Earth Pro. Though we have simplified the channel geometries, differences in stream width and streambed morphology, such as a vee-shaped channel at HC and higher

streambanks at BC, are preserved (Fig. 11).

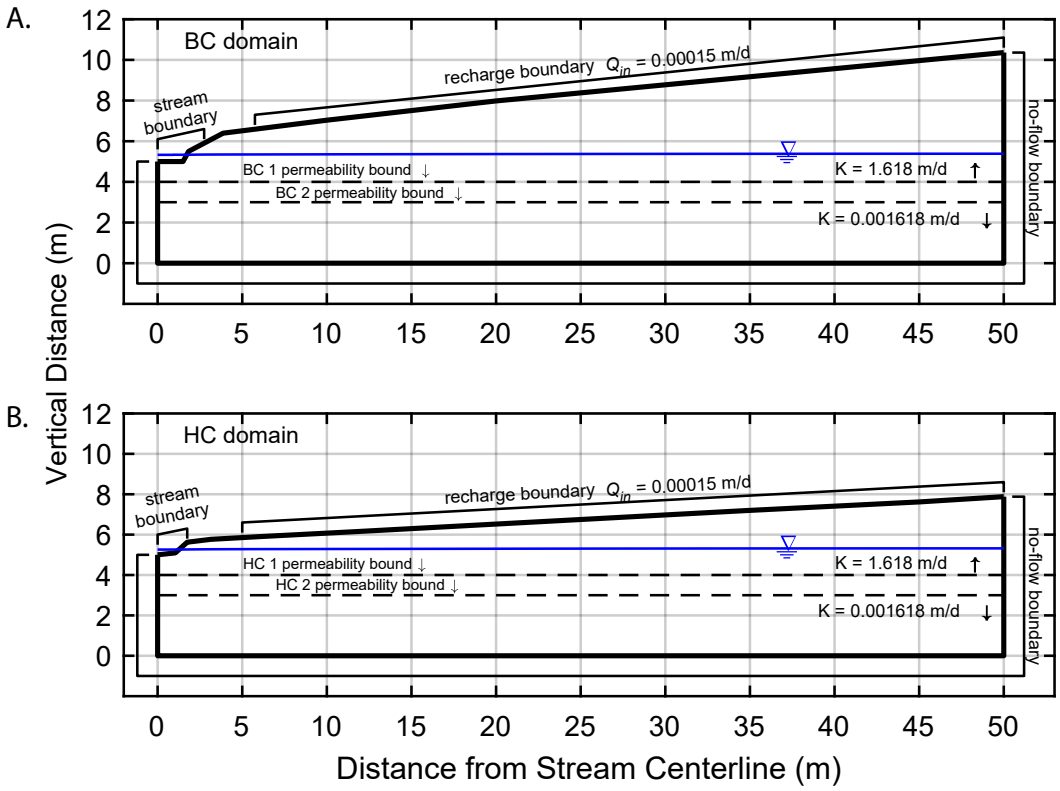

Figure 11: A) BC model domain and B) HC model domain set up. Generated stage and salinity time series were applied in the stream boundary as specified head and mass concentration boundaries, respectively.

2.5.2 Boundary and Initial Conditions

The lower and distal edges of both model domains were set as no-flow boundaries. A constant downward flux of 0.00015m/d was applied to the upper (ground surface) boundary from a distance of 3.75m from the stream bank to the far edge of the model to simulate recharge from precipitation (Fig. 11). This value was chosen in order to obtain a realistic hydraulic gradient of 0.002. Initial salinity was set to zero everywhere.

A uniform hydraulic conductivity of 0.001618m/d was applied to the lower portio of each domain to model low conductivity weathered bedrock, and a hydraulic conductivity of 1.618m/d as calculated from the grainsize distribution of floodplain sediments was

applied to the upper portion of the domain. Two scenarios were constructed at each site: one with the permeable/less permeable boundary located 1m below the lowest point of the stream bed (models BC1 and HC1), and one with the permeable/less permeable boundary located 2m below the lowest point of the streambed (BC2 and HC2) in order to investigate the effects of permeable layer thickness on salt storage and discharge. Each model was run for 10 years without applied salt or stage fluctuations to establish steady-state conditions before transient models were begun.

2.5.3 Model Runs

Model years were run from July 1 to June 30. Synthetic salinity and stage time series were generated one year at a time for each model cross section and applied as in stream boundary conditions. Generating salinity time series year-by-year allowed us to update teh baseflow salinity value as salt accumulated in the aquifer. The salinity value of the saddle in salinity contours adjacent to the stream on model day 365 was used as the new baseflow value.

For the second round of model runs with changed permeable layer thickness, the same five years of generated data were used as for the first five years of modeling at that domain, but salinity series were shifted up or down to accommodate differences in estimated baseflow salinity. If shifting the dataset down created negative salinity values, these were forced to zero.

Model outputs were saved on days 154 (beginning of winter salt season), 274 (end of winter salt season), and 365 (mid summer). Total mass of salt stored in the cross section was calculated at each observation time by integrating numerically over the model domain and assuming a transect thickness of 1 m.

3 RESULTS

3.1 Salt Plume Extent

Salt plume shape and size varied seasonally (Fig. 12), with annual maximum extent at the end of winter (model day 274) and annual minimum extent at the end of fall (model day 154). Day 154 was chosen for comparison between years and model runs, as the passage of spring, summer, and fall without additional salt inputs allowed the salt plume shape to stabilize. At this time step in the fifth model year, the 0.01‰ salinity contour had extended into the floodplain 15.1m in BC1, 14.85m in BC2, 15.17m in HC1, and 15.03m at HC2 at the elevation of the base of the streambed (Fig. 13). Maximum salinities at this time step were 0.0972‰ at BC1, 0.0978‰ at BC2, 0.0874‰ at HC1, and 0.0954‰ at HC2, and were located directly beneath the stream centerline, just below the top of the less permeable layer in all models.

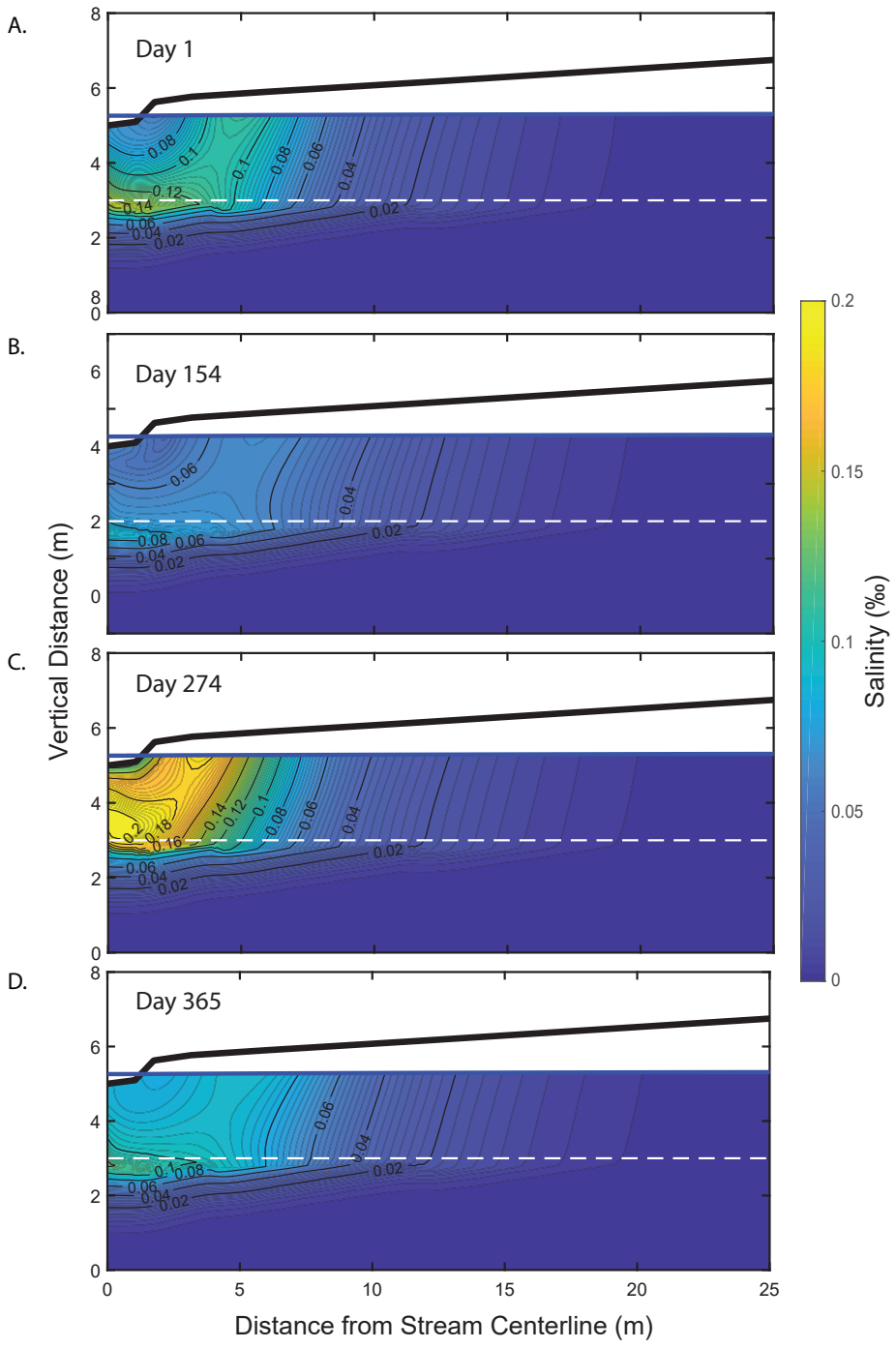

Figure 12: Model outputs from year 5 of the HC2 model A) day 0 (mid-summer), B) day 154 (end of fall), C) day 274 (end of winter), and D) day 365 (mid-summer), illustrating annual variations in groundwater salinity. Groundwater salinity is highest at the end of winter (model day 274) and lowest at the end of fall (model day 154). Intermediate times show intermediate concentrations. All panels show the effect of fresh stage fluctuation events whose associated reverse gradients push the area of maximum salinity away from the streambed.

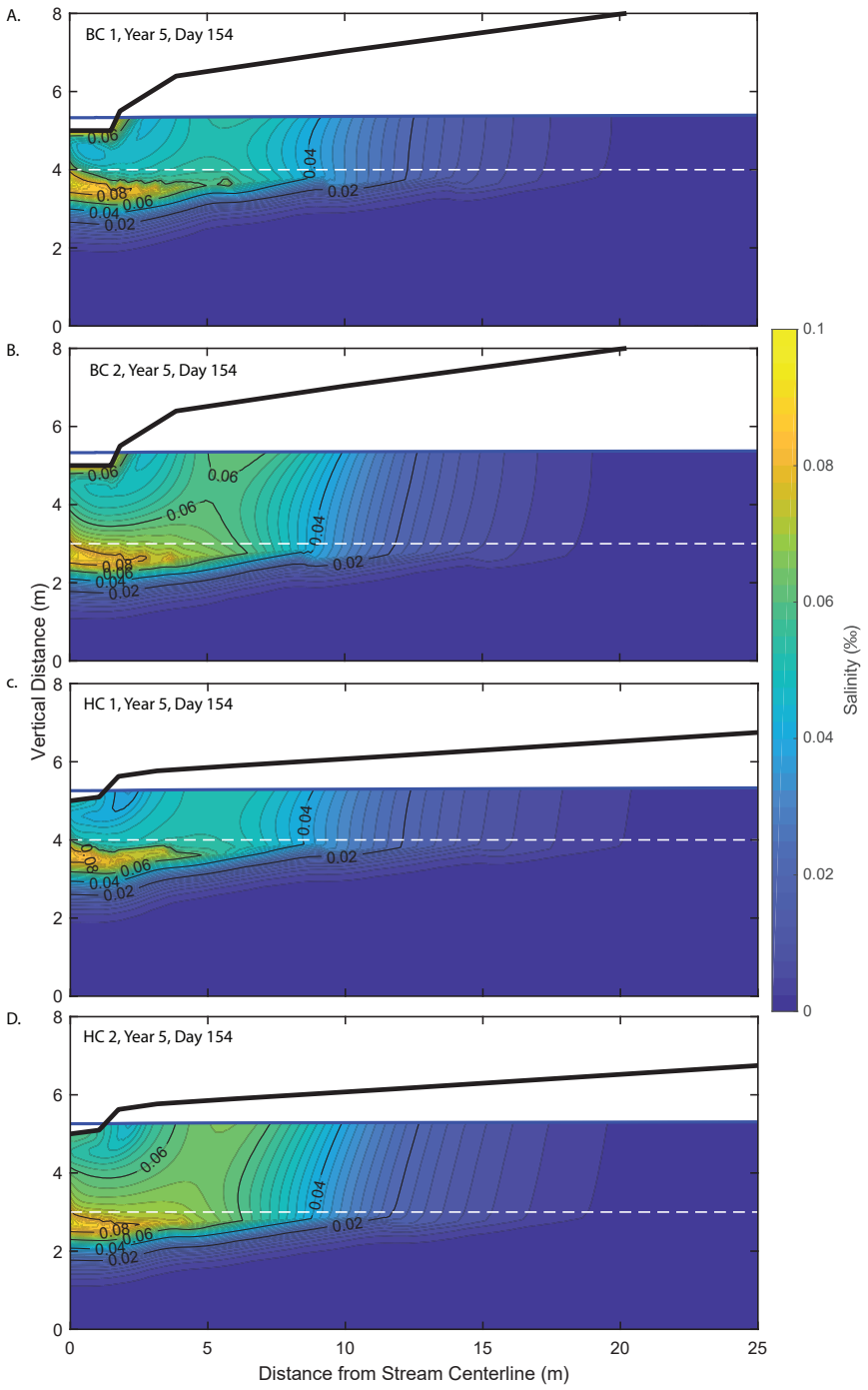

Figure 13: Contour plots showing groundwater salinity distribution at the beginning of winter in the final model year for A) the BC1 simulation, with maximum salinity of 0.097‰ and total stored salt mass of 1.42 kg, B) the BC2 simulation showing a maximum salinity of 0.097‰ and a total stored mass of 2.13 kg, C) the HC1 simulation showing maximum salinity of 0.087‰ and total stored salt mass of 1.42 kg, and D) the HC2 simulation, with a maximum salinity of 0.095‰ and a stored salt mass of 2.11 kg. The salt plume has extended furthest into the floodplain in HC1.

3.2 Total Mass Accumulation

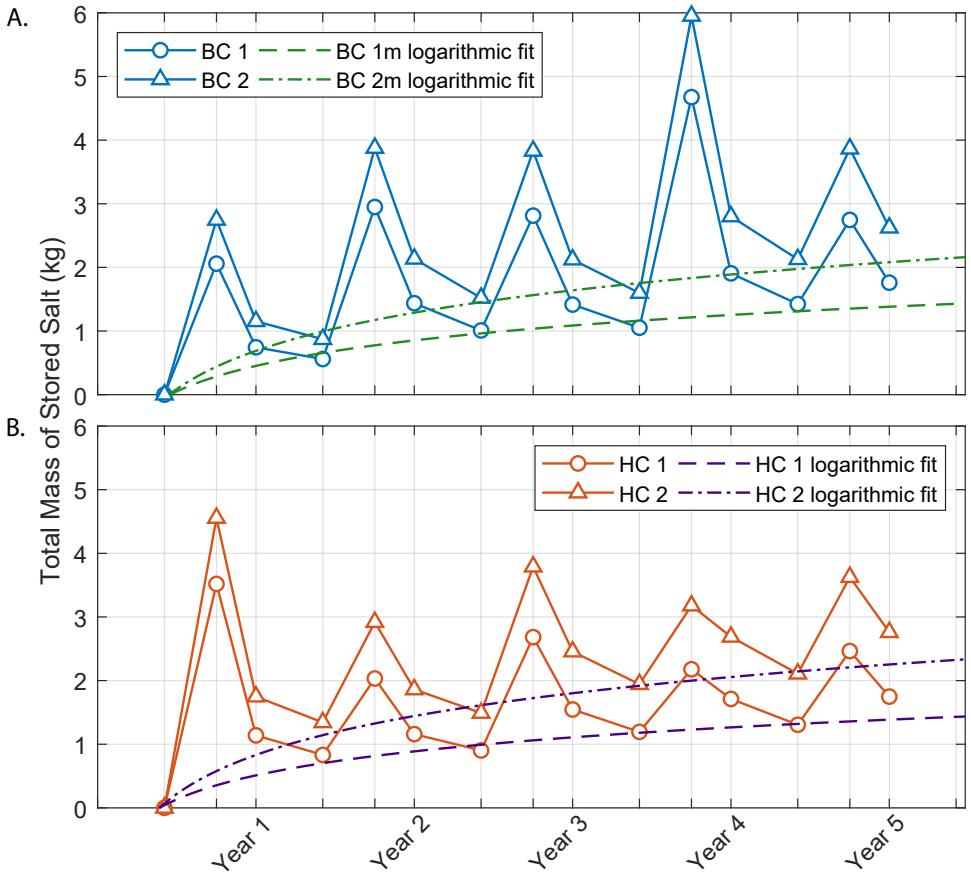

Figure 14: Total mass of salt stored in a 1 m thick extension of the modeled 2-D cross section over time at A) model site BC and B) model site HC for both permeable-layer thickness scenarios. Total mass stored fluctuates annually, with maxima at the end of winter and minima at the end of fall. Annual maxima vary with winter severity, but minima consistently increase over time in a logarithmic manner as illustrated by the dashed and dot dashed lines, which are logarithmic least squares regressions fit to the minimum annual values.

Stored mass also varied seasonally with annual maxima at the end of winter (day 274) and annual minima at the end of fall (day 154) (Fig. 14). Stored mass present on day 154 of the final model year was 1.42kg at BC1, 2.13kg at BC2, 1.31kg at HC1, and 2.15kg at HC2. Annual maximum stored salt mass varied with winter storm intensity and salinization event magnitude, but annual minima at the end of fall increased along a logarithmic trend. The minimum mass storage trendlines for HC1 and BC1 tracked each

other closely, but the HC2 and BC2 minimum mass storage trends differed by 0.17kg by the end of the five-year model period, and by 0.18kg when the logarithmic fits were projected an additional five years into the future (Fig. 15).

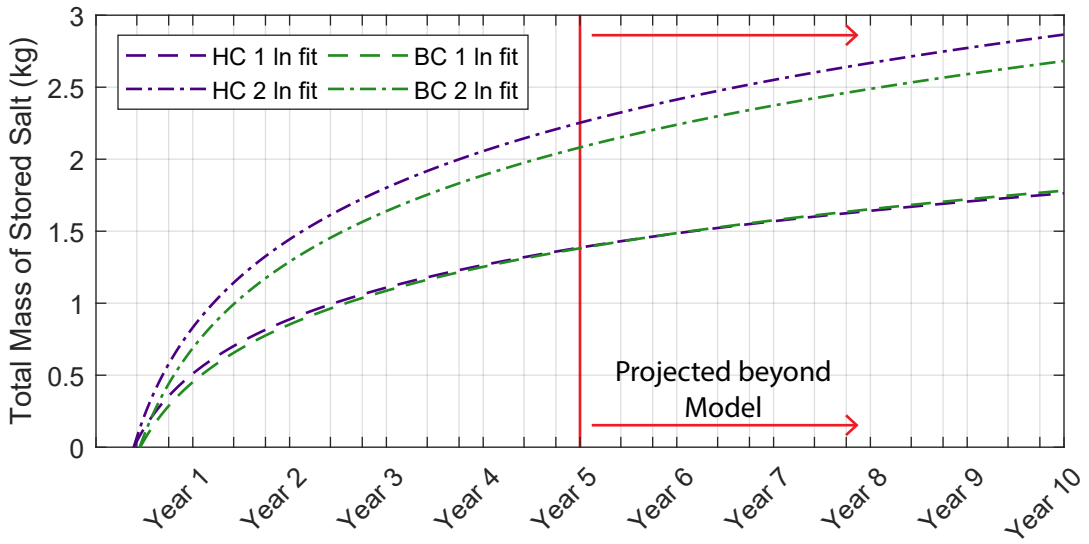

Figure 15: Comparison of the logarithmic regressions fit to the minimum annual stored salt values for each of the four model scenarios. Of interest is that the thicker permeable layer scenarios show greater difference in stored salt between the two streams.

4 DISCUSSION

4.1 Intrusion Mechanism

Previous work has suggested that near-stream aquifer salinization occurs primarily through infiltration of salty water through the floodplain, either during overbank events (Ledford et al. 2016) or from stormwater retention ponds (Snodgrass et al., 2017). Our models, which confined stage fluctuation boundary conditions to the stream channel, show that within-bank storm events, which temporarily convert the gaining stream to a losing stream, are physically capable of effectively salinizing the floodplain aquifer. The relatively steep reverse gradient of a storm event quickly drives salty stormwater into the streambanks. The hydraulic gradient feeding the stream during baseflow conditions is much flatter and cannot discharge the loaded salt nearly as quickly as it was stored.

Non-salty storms further inhibit salt flushing by pushing a layer of freshwater into the streambanks which forces salty water farther into the floodplain and creates the the saddle in salinity contours visible in figure 12.

4.2 Mass Storage

The logarithmic increase of annual minimum stored salt mass over time indicates the system becomes disproportionately more efficient at flushing salt as the concentration of salt increases, rather than the system flushing a consistent percentage of the input amount. Coupled with the fact that the trend of minimum annual stored mass over time shallows more quickly in the thinner permeable layer cases than the thicker permeable layer cases, this indicates that the thinner aquifer provides less room for the intruding salt plume to spread and dilute, forcing baseflow to have higher concentrations of salt and more effectively flushing the salt from the system. Thus increasing the thickness of the permeable layer allows an increase in stored salt mass not only because there is more space to store salt, but because that space gives the intruding salt room to disperse and dilute. A thicker permeable layer also increases the effect of stream geometry and storm dynamics on mass stored, exhibited by the larger difference in minimum mass stored after 5 years between HC2 and BC2 than between HC1 and BC1.

5 CONCLUSIONS

These models support the findings of Cockerill et al. (2017) that winter precipitation and runoff events, even when they do not lead to overbank flooding, can lead to near-stream aquifer salinization, which in turn increases year-round stream salinity as stored salty water discharges back to the stream. We additionally find the thickness of the near-stream aquifer permeable layer has a greater effect on long term total mass storage than in-stream dynamics, with larger total salt mass accumulating in thicker permeable layers, and that more salt is stored in the banks of our smaller, flashier study stream than

our larger study stream. This indicates that the greater stage fluctuation magnitude to stream size ratio during both salty and fresh events, as well as greater winter salinity spikes, produce larger and more persistent salt plumes.

Of course permeable layer thickness cannot be changed with stormwater management practices, and further research would be needed to determine whether the greater mass stored in thicker aquifer layers actually has the effect of increasing stream salinities, since there was little difference in maximum salinity between the thick and thin permeable layer scenarios. More likely, this greater stored volume and reduced export efficiency translates to longer recovery times rather than higher stream salinities in comparison to thinner aquifers.

Factors which can be affected by human practice are stage fluctuation magnitude and frequency, and volume of road salt applied to ISC. Stormwater management infrastructure which slows runoff rather than piping it directly from impervious surfaces to streams via storm drains, would reduce the magnitude of reverse hydraulic gradients. Smaller reverse gradients have less energy to force stormwater into streambanks, and would thus promote less salt plume expansion. Stormwater retention areas could assist with this, but create salt infiltration problems of their own (Snodgrass et al., 2017). The alternative strategy for reducing the salt load to the watershed is to simply apply less salt to impervious surfaces. This requires no additional stormwater management infrastructure to implement, but could be met with resistance, as winter salting has become the societal norm for winter safety in many urban areas. Suitable alternatives would need to be introduced, and these come with their own environmental considerations as well.

In regard to our second objective of determining what to expect for the future of salinity in our study streams, none of our four model scenarios, with baseflow concentration estimated by mid-summer salinity contour saddle value, reached the baseflow concentrations near 0.20‰ observed in-stream by the end of the five model years. Continued model runs will be useful in determining whether the trend in mass storage is indeed logarithmic

and in determining whether the model was well calibrated. Additional modeling planned with reduced stage fluctuations to simulate improved runoff management practices and reduced salt inputs simulating reduced road salt application rates will also be useful in determining the relative importances of storm energy and mass input in long-term stream salinization trends.

6 ACKNOWLEDGEMENTS

Appalachian State Department of Geological and Environmental Sciences (AGES)

Appalachian State University Office of Student Research

Josh Mendes, DHI software products

Anthony Love, AGES

William Armstrong, AGES

Scott Marshall, AGES

7 REFERENCES

Berezina, N.A., 2002, Tolerance of freshwater invertebrates to changes in water salinity: Russian Journal of Ecology, v. 34, p. 261-266.

Blasius, B.J., and Merritt, R.W., 2002, Field and laboratory investigations on the effects of road salt (NaCl) on stream macroinvertebrate communities: Environmental Pollution. v. 120, p.219-231.

Cockerill, K., Anderson, W.P. Jr., Harris, C., and Straka, K., 2017, Hot, salty water: A confluence of issues in managing stormwater runoff for urban streams: Journal of the American Water Resources Association, v. 53, p. 707-724.

Cooper, C.A., Mayer, P.M., and Faulkner, B.R., 2014, Effects of road salts on groundwater and surface water dynamics of sodium and chloride in an urban restored stream: Biogeochemistry, v. 121, p. 149-166.

Corsi, S.R., De Cicco, L.A., Lutz, M.A., and Hirsch, R.M., 2015, River chloride trends in snow-affected urban watersheds: increasing concentrations outpace urban growth rate and are common among all seasons: Science of the Total Environment, v. 508, p. 488-497.

Corsi, S.R., Graczyk, D.J., Geis, S.W., Booth, N.L., and Richards, K.D., 2010, A fresh look at road salt: Aquatic toxicity and water-quality impacts on local, regional, and national scales: Environmental Science and Technology, v. 44, p. 7376-7382.

Fofonoff, N.P., and Millard, R.C. Jr., 1983, Algorithms for computation of fundamental properties of seawater: Unesco Technical Papers in Marine Science 44.

Gallagher, M.T., Snodgrass, J.W., Brand, A.B., Casey, R.E., Lev, S.M, and Van Meter, R.J., 2014, The role of pollutant accumulation in determining the use of stormwater ponds by amphibians: Wetlands Ecology Management, v. 22, p. 551-564.

Godwin, K.S., Hafner, S.D., Buff, M.F., 2002, Long-term trends in sodium and chloride in the Mohawk River, New York: the effect of fifty years of road-salt application: Environmental Pollution, v. 124, p. 273-281.

Kaushal, S.S., Groffman, P.M., Likens, G.E., Belt, K.T., Stack, W.P., Kelly, V.R., Band, L.E., and Fisher, G.T., 2005, Increased salinization of freshwater in the northeastern United States: Proceedings of the National Academy of Sciences U.S.A., v. 102, p. 1351713520.

Kelly, V.R., Lovett, G.M., Weathers, K.C., Findlay, S.E.G., Strayer, D.L., Burns, D.J., and Likens, G.E., 2008, Long-term sodium chloride retention in a rural watershed: legacy effects of road salt on streamwater concentration: Environmental Science and Technology, v. 42, p. 410-415.

Kunkle, S.H., 1972, Effects of road salt on a vermont stream: Journal of the American Water Works Association, v. 64, p. 290-295.

Ledford, S.H., Lautz, L.K., and Stella, J.C., 2016, Hydrogeologic processes impacting storage, fate, and transport of chloride from road salt in urban riparian aquifers:

Environmental Science and Technology, v. 50, p. 4979-4988.

Likens, G.E., and Buso, D.C., 2009, Salinization of Mirror Lake by road salt: Water, Air and Soil Pollution, v. 205, p. 205-214.

Novotny, E.V., Sander, A.R., Mohseni, O., and Stefan, H.G., 2009, Chloride ion transport and mass balance in a metropolitan area using road salt: Water Resources Research, v. 45, W12410.

Perera, N., Gharabaghi, B., and Howard, K., 2013, Groundwater chloride response in the Highland Creek watershed due to road salt application: A re-assessment after 20 years: Journal of Hydrology, v. 479, p. 159-168.

Snodgrass, J.W., Moore, J., Lev, S.M, Casey, R.E., Ownby, D.R., Flora, R.F., and Izzo, G., 2017, Influence of modern stormwater management practices on transport of road salt to surface waters: Environmental Science and Technology, v. 51, p. 4165-4172.

United States Geological Society (USGS), 2015, Minerals yearbook: salt (advance release), accessed 4/27/2019.

US Environmental Protection Agency (USEPA), 1988, Ambient water quality criteria for chloride - February 1988.

US Environmental Protection Agency (USEPA), 2018, 2018 Edition of the drinking water standards and health advisories tables, p 10.

Wagner, E.J., Arndt, R.E., Brough, M., 2001, Comparative tolerance of four stocks of cutthroat trout to extremes in temperature, salinity, and hypoxia: Western North American Naturalist, v. 61, p. 434-444.

Williams, D.D., Williams, N.E., and Cao, Y., 2000, Road salt contamination of groundwater in a major metropolitan area and development of a biological index to monitor its impact: Water Research, v. 34, p. 127-128.